IEEE Access
Multidisciplinary ⋮ Rapid Review ⋮ Open Access Journal

Received January 2, 2020, accepted January 21, 2020, date of publication January 29, 2020, date of current version February 10, 2020.

Digital Object Identifier 10.1109/ACCESS.2020.2970206

UAV-Enabled Reliable Mobile Relaying Based on Downlink NOMA

LEI WANG[1], BO HU[1], (Member, IEEE), SHANZHI CHEN[2], (Fellow, IEEE), AND JIAN CUI[1]

[1]State Key Laboratory of Networking and Switching Technology, Beijing University of Posts and Telecommunications, Beijing 100876, China
[2]State Key Laboratory of Wireless Mobile Communication, China Academy of Telecommunication Technology, Beijing 100191, China

Corresponding author: Bo Hu (hubo@bupt.edu.cn)

This work was supported by the National Natural Science Foundation of China (NSFC) under Grant 61931005.

ABSTRACT Unmanned aerial vehicle (UAV) relaying is an efficient solution to provide wireless access for emergency communications due to the high flexibility. The system reliability is usually constrained under limited bandwidth and power resources. Downlink non-orthogonal multiple access (NOMA) can improve the system reliability through a higher resource utilization. To this end, we introduce downlink NOMA to a UAV-enabled mobile relaying system and investigate a scenario where a fixed-wing UAV flies in a circular trajectory to serve as a mobile decode-and-forward (DF) relay in an emergency situation. Since guaranteeing a reliable link is necessary in an emergency situation, our formulated problem is to minimize the maximum outage probability among all links, taking into account the bandwidth and power allocations based on downlink NOMA. Specially, the condition for successful successive interference cancellation (SIC) is also considered. By making change of variables and introducing slack variables, we reformulate our problem into a more tractable form, then we propose an iteration algorithm to solve our problem based on the successive convex optimization (SCO) technique. The optimized bandwidth and power allocation schemes as well as the min-max outage probability along the UAV trajectory are obtained, respectively. Two benchmarks are designed to reveal the performance of our proposed algorithm, and the reliability gain can be obtained by comparing the min-max outage probability and the overall average outage probability.

INDEX TERMS UAV, mobile relaying, downlink NOMA, outage probability, resource allocation.

I. INTRODUCTION

A. BACKGROUND AND MOTIVATION

Unmanned aerial vehicles (UAVs) have attracted considerable attention because of a wide range of applications [1]–[5]. Particularly, benefiting from the dominant line-of-sight (LoS) component of the air-to-ground (AtG) link [6], the UAV-enabled wireless communications promise to suffer lower propagation loss, which improves the link quality of service (QoS) performance. Thus, UAVs serving as aerial base stations (BSs) or relays are widely used to further boost the network capacity [7]–[9] or realize more flexible coverage [10]. Due to unique structural features, fixed-wing UAVs are usually used as mobile BSs or relays to provide dynamic connectivity from the sky. In addition to mobility, rotary-wing UAVs can also keep still to provide a quasi-static wireless propagation channel. Thanks to the high flexibility of UAVs, both two kinds of UAVs can accomplish on-demand and cost-effective deployments [11]. Attracted by above reasons, UAVs have been widely applied to many communication scenarios, especially in an emergency situation to provide wireless access for users in danger [12]–[16].

UAVs used in an emergency situation usually work as relays since they need to provide backhaul links to realize information exchange [16]. Compared with a ground relay, a UAV relay is more efficient. Firstly, a ground relay that is temporarily deployed in a disaster area may be destroyed once again due to a harsh environment. Whereas a UAV relay is free from the ground damage due to its high altitude. Secondly, a higher UAV altitude provides a better LoS propagation channel, which makes the AtG link enjoy the Rician fading channel instead of the Rayleigh fading channel dominated in the ground link, and thus improves the channel performance. Therefore, a UAV serving as an aerial relay is more suitable to temporarily provide communication services in an emergency situation.

Because an emergency communication link provides necessary services for users in danger, how to guarantee

The associate editor coordinating the review of this manuscript and approving it for publication was Zhenyu Xiao.

reliable relaying under a limited communication resource is an important issue. Downlink non-orthogonal multiple access (NOMA) allows simultaneous transmission among multiple links with the same frequency, which can improve the bandwidth utilization by carefully designing the communication resource, and thus is suitable to further improve the reliability for resource-limited UAV relaying systems in emergency communications. Motivated by this reason, this paper considers a downlink NOMA-assisted UAV relaying system, providing wireless access for emergency communications in a disaster area. We aim to optimize the link outage probability with a given communication resource to guarantee reliable relaying.

B. RELATED WORKS

The works in [17]–[20] assumed a UAV as a mobile decode-and-forward (DF) relay, flying in a circular trajectory. Specifically, Ono *et al.* in [17] proposed a variable-rate relaying approach to optimize the time allocation scheme, and they compared the outage probability with the fixed-rate case; Jiang *et al.* in [18] developed the optimal time and power allocation schemes to minimize the average outage probability for Rayleigh fading and Rician fading channels, respectively; Song *et al.* in their works [19] and [20] optimized the beamforming and power allocation to maximize the end-to-end signal-to-noise ratio (SNR) for half-duplex and full-duplex, respectively, then they derived the closed outage probability expression to investigate the reliability gain. Yuan *et al.* in [21] developed the location-based beamforming scheme to improve the secrecy outage performance. The UAV trajectory and power allocation were jointly designed to improve the global reliability in [22]–[24]. Note that the works in [17]–[24] mainly focus on the time and power resources or beamforming for mobile relaying systems. The bandwidth resource that significantly affects the channel capacity and noise level is not considered. Besides, these works in [17]–[24] assume a source node communicates with a destination node via a UAV relay, where the co-channel interference does not exist.

For multi-link communication systems, NOMA actively introduces the co-channel interference through reusing the bandwidth resource, which is able to improve the resource utilization by the successive interference cancellation (SIC) technique. Sharma and Kim [25] gave a theoretical outage analysis on a UAV-assisted downlink two-user NOMA system. Selim *et al.* [26] considered a UAV-assisted device-to-device (D2D) communication scenario and derived the link outage probability based on downlink two-user NOMA. Han *et al.* [27] applied downlink NOMA to the UAV with consideration of a imperfect SIC to analyze the link outage probability. Hou *et al.* [28] investigated a multi-antenna UAV communication scenario with downlink NOMA and derived the analytical outage probability by a stochastic geometry approach. Wang *et al.* [29] assumed a multi-node AtG cooperative NOMA network to analyze the system outage performance. Li *et al.* [30] considered a dual-UAV-enabled NOMA relaying system and analyzed the uplink, downlink and overall outage probabilities, respectively. Except for [30], the backhaul links are not considered in [25]–[29]. Moreover, all the works in [25]–[30] assume a pre-defined resource allocation scheme without resource optimization, which in fact increases the impact of the co-channel interference on the system reliability and reduces the resource utilization, since the co-channel interference can be mitigated by careful resource optimization [31], [32].

C. CONTRIBUTIONS

In this paper, we consider an emergency communication scenario where multiple access points (APs) without backhaul links are left in a disaster area. We assume that a UAV flies in a circular trajectory to provide relaying services between multiple remote BSs and these remaining APs. Downlink NOMA is applied to the UAV for a higher resource utilization. Compared with orthogonal transmission, the co-channel interference introduced by downlink NOMA weakens the system reliability. How to optimize the bandwidth and power allocations to improve the system reliability remains to be a meaningful issue. To this end, we give a joint design of the bandwidth and power allocations along the UAV trajectory to minimize the maximum outage probability among all links. Our main contributions of this paper are given as follows:

- By using the DF relaying protocol, a UAV-enabled mobile relaying system based on downlink NOMA is established, forwarding information from multiple remote BSs to multiple remaining APs in an emergency situation. With consideration of the co-channel interference introduced by downlink NOMA, the bandwidth and power allocations are jointly designed along the UAV trajectory to obtain the min-max outage probability among all links.
- With the aid of variable substitutions and slack variables, we deal with our formulated problem by converting it into a more tractable form. Then, an iteration algorithm based on the successive convex optimization (SCO) technique is proposed to solve our problem.
- The optimized bandwidth and power allocation schemes are developed along the UAV trajectory, respectively. The min-max outage probability along the UAV trajectory is also given. A lower min-max outage probability can be obtained when the largest bandwidth resource is allocated to the second hops. The min-max outage probability along the UAV trajectory based on downlink NOMA is lower than that based on downlink orthogonal multiple access (OMA). Our proposed algorithm also obtains the reliability gain by comparing the overall average outage probability.

D. ORGANIZATION

The rest of this paper is organized as follows. Section II gives our formulated outage probability optimization problem. In Section III, our proposed iteration algorithm based on the SCO technique is given. Simulation results are presented

in Section IV, followed by the conclusion of this paper in Section V.

II. SYSTEM MODEL AND PROBLEM FORMULATION

As shown in the right side of Figure 1, we consider a ground region where a two-tier heterogeneous network (HetNet) is initially deployed, i.e., multiple APs such as micro-BSs that provide wireless coverage on high user-density areas and a macro-BS that provides backhaul links for these APs. In an emergency situation such as earthquake, we assume that the macro-BS is broken, only with N APs left. A traditional way to recover the network connection is to use emergency communication vehicles, which is inefficient and time-consuming due to the disaster. Thanks to the fast development of electronics and energy technologies, utilizing UAVs to assist communications has attracted much attention. A fixed-wing UAV is more power-saving and has a larger battery capacity [33], [34], which can bring a longer battery life. Therefore, we assume a fixed-wing UAV denoted by u as an aerial mobile relay, providing communication links between the remote BSs (the left side of Figure 1) and the APs. These remaining APs in the emergency area are out of the coverage of remote BSs, thus only the UAV relay can be used to forward information to provide communication services. Since each remote BS needs to provide local services, we further assume that each remote BS can only provide additional access for one AP. Thus, N remote BSs are used to provide backhaul links. The information from BS s_i ($i \in \{1, 2, \ldots, N\}$) is forwarded to corresponding AP d_i via UAV relay u. This is actually a communication pre-matching process for load balancing, and can be pre-executed by the communication service provider according to the load of remote BSs. We take the link s_i–u–d_i as link i.

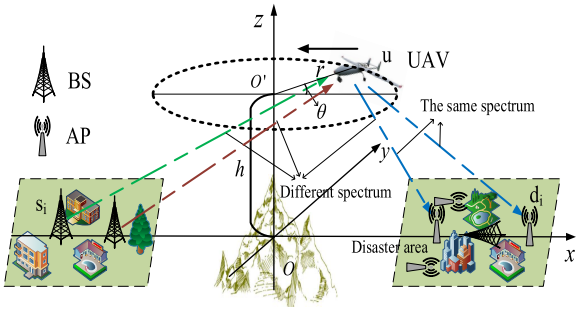

FIGURE 1. A UAV-enabled mobile relaying system based on downlink NOMA.

Without loss of generality, (x_{s_i}, y_{s_i}) and (x_{d_i}, y_{d_i}) are defined as the coordinates of remote BS s_i and AP d_i, respectively. Similar with [17]–[20], we consider that the UAV flies in a circular trajectory with the circle center of O' and the circle radius of r. The coordinate of O' is $(0, 0, h)$, where h represents the UAV flying altitude. θ $(0 \le \theta \le 2\pi)$ is defined as the azimuth angle of UAV along the circle. Therefore, the UAV trajectory can be represented by $(x_u, y_u, h) = (r\cos(\theta), r\sin(\theta), h)$. The Euclidean distances between BS s_i or AP d_i and the UAV are written as:

$$d_{s_iu} = \sqrt{(x_{s_i} - x_u)^2 + (y_{s_i} - y_u)^2 + h^2}, \tag{1}$$

$$d_{ud_i} = \sqrt{(x_{d_i} - x_u)^2 + (y_{d_i} - y_u)^2 + h^2}. \tag{2}$$

We assume that the UAV relay works in the frequency division duplexing (FDD) mode so that the information received from the remote BSs can be real-time forwarded to the APs. The BSs and APs are assumed to be equipped with a single antenna. For the UAV, one antenna is used to receive information from N uplinks with frequency division multiple access (FDMA) (different colors in the first hops); the downlinks share the same bandwidth resource by using downlink NOMA (the same color in the second hops), where another antenna is used to transmit information to the APs. Thus, the co-channel interference is introduced by using downlink NOMA. P_{s_i} is the transmit power of BS s_i. P_{u_i} denotes the allocated power from the UAV for link ud_i. To efficiently utilize the power resource, we further consider a power-limited communication system. $P_{\max}$ is defined as the maximum allowed total transmit power in this communication system. For a given $P_{\max}$, we obtain $P_{s_i} = P_{\max}\xi_{s_i}$ and $P_{u_i} = P_{\max}\xi_{u_i}$, where ξ_{s_i} and ξ_{u_i} are the power allocation coefficients for P_{s_i} and P_{u_i}, respectively. Since $\sum_{i=1}^{N} P_{s_i} + \sum_{i=1}^{N} P_{u_i} \le P_{\max}$, we have the following relations:

$$\sum_{i=1}^{N} \xi_{s_i} + \sum_{i=1}^{N} \xi_{u_i} \le 1, \tag{3}$$

$$0 \le \xi_{u_i} \le 1, 0 \le \xi_{s_i} \le 1, \quad \forall i. \tag{4}$$

Besides, B_t represents the total system bandwidth. β_{s_iu} is the bandwidth allocation coefficient for the first hop s_iu of link i, and $B_t\beta_{s_iu}$ is the allocated bandwidth for BS s_i to transmit information to the UAV. β_{ud} is the bandwidth allocation coefficient for the second hops, and $B_t\beta_{ud}$ is the shared bandwidth for the second hops to transmit information to the APs by using downlink NOMA. Since the total allocated bandwidth can not exceed the total allowed system bandwidth, the following constraints hold:

$$\beta_{ud} + \sum_{i=1}^{N} \beta_{s_iu} \le 1, \tag{5}$$

$$0 \le \beta_{ud} \le 1, 0 \le \beta_{s_iu} \le 1, \quad \forall i. \tag{6}$$

Since the AtG link usually contains a strong LoS component and some other multi-path components, the Rician channel proposed by [35] is used to model the AtG link. The Rician factor and path loss exponent of the AtG link are related to the elevation angle. The elevation angle of the AtG link in radian can be obtained by:

$$\Theta_{mn} = \sin^{-1}\left(\frac{h}{d_{mn}}\right), \quad mn \in \{s_iu, ud_i\}. \tag{7}$$

According to [35], the Rician factor and path loss exponent can be respectively modeled as:

$$K_{mn} = a_1 \exp(b_1\Theta_{mn}), \tag{8}$$

$$\alpha_{mn} = \frac{a_2}{1 + a_3 \exp(-b_3 \Theta_{mn})} + b_2, \quad (9)$$

where a_1, b_1, a_2, b_2, a_3 and b_3 are constant parameters and mainly depend on the environment.

Let h_{mn} be the small-scale fading gain of link mn used in the Rician fading channel. According to [35], $|h_{mn}|^2$ satisfies the non-central chi-square distribution. The probability distribution function (PDF) of $|h_{mn}|^2$ can be expressed as [35]:

$$f_{|h_{mn}|^2}(t) = \frac{(1+K_{mn})\exp(-K_{mn})}{\bar{A}} \times \exp(-\frac{(1+K_{mn})t}{\bar{A}}) I_0(2\sqrt{\frac{K_{mn}(1+K_{mn})t}{\bar{A}}}), \quad (10)$$

where $\bar{A} = 1$ denotes the average power of $|h_{mn}|^2$ and $I_0(.)$ is the zero-order modified Bessel function of the first kind. Therefore, the cumulative density function (CDF) of $|h_{mn}|^2$ can be expressed as [35]:

$$F_{|h_{mn}|^2}(t) = P(|h_{mn}|^2 \le t) = \int_0^t f_{|h_{mn}|^2}(t)dt = 1 - Q_1(\sqrt{2K_{mn}}, \sqrt{2(1+K_{mn})t}), \quad (11)$$

where $Q_1(.,.)$ is the first-order Marcum Q-function defined by:

$$Q_1(a,b) = \int_b^{+\infty} x \exp(-\frac{x^2+a^2}{2}) I_0(ax)dx. \quad (12)$$

Based on the above derivations, the instantaneous transmission rate of link s_iu can be formulated as:

$$R_{s_iu} = B_t \beta_{s_iu} \log_2(1 + \frac{P_{\max}\xi_{s_i} d_{s_iu}^{-\alpha_{s_iu}} |h_{s_iu}|^2}{B_t \beta_{s_iu} N_0}), \quad \forall i, \quad (13)$$

where N_0 is the noise power spectral density, and $B_t\beta_{s_iu}N_0$ represents the additive noise power of link s_iu; $d_{s_iu}^{-\alpha_{s_iu}}$ represents the large-scale fading gain of link s_iu; $|h_{s_iu}|^2$ represents the small-scale fading gain of link s_iu.

Once the link transmission rate is lower than a rate threshold R_{th}, this communication link is considered to be interrupted. According to (11) and (13), one can formulate the outage probability of link s_iu as:

$$P_{s_iu} = P[R_{s_iu} < R_{th}] = P[|h_{s_iu}|^2 < E_{s_iu}] = 1 - Q_1(\sqrt{2K_{s_iu}}, \sqrt{2(1+K_{s_iu})E_{s_iu}}), \quad \forall i, \quad (14)$$

where E_{s_iu} is derived as:

$$E_{s_iu} = \frac{(2^{\frac{R_{th}}{B_t\beta_{s_iu}}} - 1) B_t \beta_{s_iu} N_0}{P_{\max}\xi_{s_i} d_{s_iu}^{-\alpha_{s_iu}}}, \quad \forall i. \quad (15)$$

For the second hops, according to the SIC technique in downlink NOMA, the signals received by the links with higher channel gains can cancel the co-channel interferences from other links with lower channel gains. Without loss of generality, the channel gain is assumed to be ordered by the APs' distances from the UAV, i.e., a shorter distance brings a better channel gain.

Lemma 1: Assume $d_{ud_m} > d_{ud_i}$ for $\forall m, i \in \{1, \ldots, N\}$. Define a node set as $G_i = \{\forall g | d_{ud_i} > d_{ud_g}\}$. The outage probability of link ud_i with consideration of successful SIC can be calculated as:

$$P_{ud_i} = 1 - Q_1(\sqrt{2K_{ud_i}}, \sqrt{2(1+K_{ud_i})E_{ud_i}}), \quad \forall i, \quad (16)$$

where E_{ud_i} is calculated as:

$$E_{ud_i} = \max[\frac{(2^{\frac{R_{th}}{B_t\beta_{ud}}} - 1) B_t \beta_{ud} N_0}{P_{\max} d_{ud_i}^{-\alpha_{ud_i}} (\xi_{u_v} - (2^{\frac{R_{th}}{B_t\beta_{ud}}} - 1) \sum_{j \in G_v} \xi_{u_j})}, \quad \forall v \in \{\forall m \cup i\}], \quad \forall i, \quad (17)$$

satisfying the following successful SIC condition:

$$\xi_{u_v} - (2^{\frac{R_{th}}{B_t\beta_{ud}}} - 1) \sum_{j \in G_v} \xi_{u_j} \ge 0, \quad \forall v, \ \forall i. \quad (18)$$

Proof: Based on the channel gain order and the SIC rules, AP d_i firstly detects the signal that is useful for AP d_m and removes it from the received signal of AP d_i. According to [36], [37], the instantaneous rate of AP d_i to detect the signal for AP d_m is calculated as:

$$R_{ud_i \to ud_m} = B_t \beta_{ud} N_0 \log_2(1 + \frac{P_{\max}\xi_{u_m} d_{ud_i}^{-\alpha_{ud_i}} |h_{ud_i}|^2}{\sum_{\forall j \in G_m} P_{\max}\xi_{u_j} d_{ud_i}^{-\alpha_{ud_i}} |h_{ud_i}|^2 + B_t\beta_{ud}N_0}), \quad \forall m, \ \forall i. \quad (19)$$

The instantaneous rate of AP d_i to detect its own signal is calculated as:

$$R_{ud_i \to ud_i} = B_t \beta_{ud} N_0 \log_2(1 + \frac{P_{\max}\xi_{u_i} d_{ud_i}^{-\alpha_{ud_i}} |h_{ud_i}|^2}{\sum_{j \in G_i} P_{\max}\xi_{u_j} d_{ud_i}^{-\alpha_{ud_i}} |h_{ud_i}|^2 + B_t\beta_{ud}N_0}), \quad \forall i. \quad (20)$$

In order to guarantee that link ud_i is not interrupted, both the condition to successfully detect the signal for AP d_m and the rate requirement at AP d_i should be considered. Define the same E_{ud_i} as used in (17). Therefore, the outage probability of link ud_i is given by [36], [37]:

$$P_{ud_i} = 1 - P[\underbrace{\cap^{\forall m}(R_{ud_i \to ud_m} \ge R_{th})}_{\text{successful SIC}} \cap \underbrace{(R_{ud_i \to ud_i} \ge R_{th})}_{\text{rate requirement of link } ud_i}] \overset{a}{=} 1 - P[|h_{ud_i}|^2 \ge E_{ud_i}] \overset{b}{=} P[|h_{ud_i}|^2 < E_{ud_i}] \overset{c}{=} 1 - Q_1(\sqrt{2K_{ud_i}}, \sqrt{2(1+K_{ud_i})E_{ud_i}}), \quad \forall i, \quad (21)$$

where (a) is obtained according to (17) and (19); (c) holds according to (11); (b) holds under the premise that constraint (18) is satisfied. The proof of Lemma 1 is completed. ■

In this paper, we assume that the UAV relay works in the DF relaying mode. Thus, the outage probability of link i can

be written as:

$$\begin{aligned} P_{i,out} &= 1-(1-P_{s_iu})(1-P_{ud_i}) \\ &= 1-Q_1(\sqrt{2K_{s_iu}}, \sqrt{2(1+K_{s_iu})E_{s_iu}}) \\ &\quad \times Q_1(\sqrt{2K_{ud_i}}, \sqrt{2(1+K_{ud_i})E_{ud_i}}), \quad \forall i. \end{aligned} \tag{22}$$

By defining η as the maximum outage probability among all links, i.e., $\eta = \max\{P_{i,out}, \forall i\}$, we have the following constraint:

$$\eta \geq P_{i,out}, \quad \forall i. \tag{23}$$

Since the UAV flies in a circular trajectory, the channel is time-varying with respect to the UAV azimuth angle θ. For any given UAV location, which means a given θ, the channel gains in the second hops depend on the distances between the UAV and APs. According to the assumption in Lemma 1, we derive the link outage probability of each second hop by downlink NOMA with a priori channel gain order. Thus, with a given UAV location, the channel gain order should be firstly built according to the distance order of the second hops. Based on this channel gain order, the time-varying outage probability for each link is obtained by (22). Along the UAV trajectory, our goal is to jointly design the bandwidth allocation $\boldsymbol{\beta} = \{\beta_{s_iu}, \forall i\} \bigcup \beta_{ud}$ and power allocation $\boldsymbol{\xi} = \{\xi_{s_i}, \xi_{u_i}, \forall i\}$ to obtain the min-max outage probability among all links. Mathematically speaking, this problem can be formulated as:

$$\min_{\boldsymbol{\xi},\boldsymbol{\beta},\eta} \ \eta \tag{24a}$$

$$s.t. \ (3)\text{-}(6), \ (18) \text{ and } (23). \tag{24b}$$

Due to the existence of the first-order Marcum Q-function, the outage probability function is hard to handle. Moreover, the co-channel interference introduced by downlink NOMA makes the outage probability function highly coupled with the bandwidth and power variables. Finally, the successful SIC constraint is also related to the bandwidth and power allocations. Thus, problem (24) is a non-convex problem and hard to directly solve.

III. ALGORITHM DESIGN

To make the outage probability function more tractable, as used in [17], [18], [25], we approximate the outage probability function at a high reference SNR range. $\lambda_r = \frac{P_{\max}}{B_t N_0}$ is defined as a reference SNR. With $\lambda_r \to +\infty$, we have $\frac{1}{\lambda_r} \to 0$, and we use the Maclaurin series with respect to $l = \frac{1}{\lambda_r}$ for (22). As a result, $P_{i,out}$ can be rewritten as:

$$P_{i,out} = \sum_{n=0}^{\infty} c_n l^n, \quad \forall i, \tag{25}$$

where $c_n = \frac{\partial^n P_{i,out}}{n! \partial l^n}|_{l=0}$. $c_n l^n$ for $n \geq 2$ is the high-order infinitesimal of $c_1 l$ at the high λ_r range. Omit the high-order terms, and $P_{i,out}$ can be replaced by its first-order asymptotic value as follows:

$$P_{i,out} = c_0 + c_1 l, \quad \forall i. \tag{26}$$

According to (26), the approximation error between the first-order asymptotic outage probability and the original outage probability is $\sum_{n=2}^{\infty} c_n l^n$. For a high enough SNR λ_r, this approximation error can be ignored due to $l \to 0$. A lower reference SNR λ_r means a higher l, which brings a larger approximation error. A feasible way to cope with this problem is to firstly design the resource allocation by using the first-order asymptotic outage probability, then the original outage probability can be obtained by (22) based on the optimized resource allocation scheme. In fact, for a normal communication system setup such as $P_{\max} = 10\ w$, $B_t = 5\ M$ and $N_0 = -174\ dBm/Hz$ used in our simulations, the reference SNR is $\lambda_r = \frac{P_{\max}}{B_t N_0} \approx 5.024 \times 10^{14}$, which is high enough to get a very small approximation error. Note that the following simulation results in Section IV will also show the high accuracy by using the first-order asymptotic outage probability.

By calculation, we have $c_0 = 0$ and $c_1 = \frac{E_{s_iu}}{l}(1+K_{s_iu})\exp(-K_{s_iu}) + \frac{E_{ud_i}}{l}(1+K_{ud_i})\exp(-K_{ud_i})$. Therefore, $P_{i,out}$ is rewritten as:

$$P_{i,out} = L_{1,i}F_{1,i} + L_{2,i}F_{2,i}, \quad \forall i, \tag{27}$$

where

$$L_{1,i} = \frac{(1+K_{s_iu})\exp(-K_{s_iu})}{\lambda_r d_{s_iu}^{-\alpha_{s_iu}}}, \quad \forall i, \tag{28}$$

$$F_{1,i} = \frac{(2^{\frac{R_{th}}{B_t \beta_{s_iu}}} - 1)\beta_{s_iu}}{\xi_{s_i}}, \quad \forall i, \tag{29}$$

$$L_{2,i} = \frac{(1+K_{ud_i})\exp(-K_{ud_i})}{\lambda_r d_{ud_i}^{-\alpha_{ud_i}}}, \quad \forall i, \tag{30}$$

$$F_{2,i} = \max[\frac{(2^{\frac{R_{th}}{B_t \beta_{ud}}} - 1)\beta_{ud}}{\xi_{u_v} - (2^{\frac{R_{th}}{B_t \beta_{ud}}} - 1)\sum_{j \in G_v} \xi_{u_j}}, \forall v], \quad \forall i. \tag{31}$$

$L_{1,i}$ and $L_{2,i}$ are functions of the azimuth angle θ, which implies that $L_{1,i}$ and $L_{2,i}$ account for the time-varying channel. $F_{1,i}$ and $F_{2,i}$ depend on the optimization variables, i.e., bandwidth allocation and power allocation.

Although $P_{i,out}$ is approximated by a more tractable form in (27), $P_{i,out}$ is still non-convex with respect to $\boldsymbol{\xi}$ and $\boldsymbol{\beta}$. Specifically, $F_{1,i}$ has been proven to be jointly convex with respect to β_{s_iu} and ξ_{s_i} by [18]. However, $F_{2,i}$ is not jointly convex with respect to β_{ud}, ξ_{u_v} and ξ_{u_j} due to the interference term. Moreover, the constraint in (18) for successful SIC is also non-convex. For the proof, please refer to Appendix. Thus, problem (24) with using the first-order asymptotic outage probability is still a non-convex optimization problem. In the following, we use the SCO technique to deal with problem (24). Specially, although $F_{1,i}$ is convex, it does not satisfy the disciplined convex program (DCP) rules [38], thus can not be recognized by the existing convex optimization toolbox CVX. To efficiently solve problem (24) by CVX, we equivalently change the original problem into a more tractable form.

Without loss of optimality, we firstly make change of variables as follows:

$$s_{s_iu} = 2^{\frac{R_{th}}{B_t \beta_{s_iu}}} - 1, \quad \forall i, \tag{32}$$

$$s_{ud} = 2^{\frac{R_{th}}{B_t \beta_{ud}}} - 1, \tag{33}$$

$$t_{u_i} = \frac{1}{\xi_{u_i}^2}, \quad \forall i. \tag{34}$$

Thus, by defining the sets $\boldsymbol{s} = \{s_{s_iu}, \forall i\} \bigcup s_{ud}$, $\boldsymbol{t} = \{t_{u_i}, \forall i\}$ and $\boldsymbol{\tau} = \{\xi_{s_i}, \forall i\}$, problem (24) is equivalently transformed as:

$$\min_{\boldsymbol{s},\boldsymbol{t},\boldsymbol{\tau},\eta} \ \eta \tag{35a}$$

$$s.t. \ \sum_{i=1}^{N} \xi_{s_i} + \sum_{i=1}^{N} \frac{1}{\sqrt{t_{u_i}}} \le 1, \tag{35b}$$

$$0 \le \xi_{s_i} \le 1, \quad t_{u_i} \ge 1, \ \forall i, \tag{35c}$$

$$\frac{R_{th}}{B_t \log_2(1+s_{ud})} + \sum_{i=1}^{N} \frac{R_{th}}{B_t \log_2(1+s_{s_iu})} \le 1, \tag{35d}$$

$$s_{s_iu} \ge 2^{\frac{R_{th}}{B_t}} - 1, s_{ud} \ge 2^{\frac{R_{th}}{B_t}} - 1, \quad \forall i, \tag{35e}$$

$$\frac{1}{\sqrt{t_{u_v}}} - \sum_{j \in G_v} \frac{s_{ud}}{\sqrt{t_{u_j}}} \ge 0, \quad \forall v, \ \forall i, \tag{35f}$$

$$\eta \ge L_{1,i} \frac{\frac{R_{th} s_{s_iu}}{B_t \log_2(1+s_{s_iu})}}{\xi_{s_i}} + L_{2,i} \times \max[\frac{\frac{R_{th} s_{ud}}{B_t \log_2(1+s_{ud})}}{\frac{1}{\sqrt{t_{u_v}}} - \sum_{j \in G_v} \frac{s_{ud}}{\sqrt{t_{u_j}}}}, \forall v], \quad \forall i. \tag{35g}$$

To tackle problem (35), we further introduce slack variables $\boldsymbol{\pi} = \{\pi_{u_i}, \forall i\}$ and $\boldsymbol{\phi} = \{\phi_{s_iu}, \forall i\} \bigcup \phi_{ud}$ satisfying the following constraints:

$$\pi_{u_v} \le \frac{1}{\sqrt{t_{u_v}}} - \sum_{j \in G_v} \frac{s_{ud}}{\sqrt{t_{u_j}}}, \forall v, \quad \forall i, \tag{36}$$

$$\phi_{s_iu}^2 \ge \frac{R_{th} s_{s_iu}}{B_t \log_2(1+s_{s_iu})}, \ \forall i, \tag{37}$$

$$\phi_{ud}^2 \ge \frac{R_{th} s_{ud}}{B_t \log_2(1+s_{ud})}, \tag{38}$$

$$\pi_{u_i} \ge 0, \quad \phi_{s_iu} \ge 0, \ \phi_{ud} \ge 0, \ \forall i. \tag{39}$$

With the aid of the constraints in (36), (37) and (38), the constraint in (35g) can be equivalently replaced by:

$$\eta \ge L_{1,i} \frac{\phi_{s_iu}^2}{\xi_{s_i}} + L_{2,i} \max[\frac{\phi_{ud}^2}{\pi_{u_v}}, \forall v], \quad \forall i. \tag{40}$$

One can verify that the minimum value of η is obtained when $\pi_{u_v} = \frac{1}{\sqrt{t_{u_v}}} - \sum_{j \in G_v} \frac{s_{ud}}{\sqrt{t_{u_j}}}$, $\phi_{s_iu}^2 = \frac{R_{th} s_{s_iu}}{B_t \log_2(1+s_{s_iu})}$ and $\phi_{ud}^2 = \frac{R_{th} s_{ud}}{B_t \log_2(1+s_{ud})}$. Besides, since π_i is non-negative, the constraint in (36) holds means that the constraint in (35f) is always satisfied. Thus, problem (24) can be equivalently transformed as:

$$\min_{\boldsymbol{s},\boldsymbol{t},\boldsymbol{\tau},\boldsymbol{\pi},\boldsymbol{\phi},\eta} \ \eta \tag{41a}$$

$$s.t. \ (35b)\text{-}(35e), (36)\text{-}(40). \tag{41b}$$

The objective η and the constraints in (35b), (35c), (35d), (35e) and (39) are convex. $\max[\frac{\phi_{ud}^2}{\pi_{u_v}}, \forall v]$ in constraint (40) is the point-by-point maximum of multiple quadratic-over-linear functions. Thus, constraint (40) is also convex. Using the SCO technique, we only need to deal with the constraints in (36), (37) and (38).

Lemma 2: Define $f(x) = \frac{x}{\log_2(1+x)}$. $f(x)$ is concave with respect to $x \ge 0$.

Proof: According to $f(x)$, we have:

$$\frac{d^2 f(x)}{dx^2} = \frac{g(x) \ln 2}{(1+x)^2 (\ln(1+x))^3}, \tag{42}$$

where $g(x) = 2x - (x+2)\ln(1+x)$. The first and second derivatives of $g(x)$ are calculated as:

$$\frac{dg(x)}{dx} = 2 - \ln(1+x) - \frac{2+x}{1+x}, \tag{43}$$

$$\frac{d^2 g(x)}{dx^2} = -\frac{x}{(1+x)^2}. \tag{44}$$

$\frac{d^2 g(x)}{dx^2} \le 0$ for $x \ge 0$, which means that $\frac{dg(x)}{dx}$ is non-increasing with respect to $x \ge 0$. The maximum value of $\frac{dg(x)}{dx}$ can be obtained by $\frac{dg(x)}{dx}|_{x=0} = 0$. As a result, $g(x)$ is also non-increasing with respect to $x \ge 0$, and the maximum value of $g(x)$ is $g(x)|_{x=0} = 0$. Thus, $\frac{d^2 f(x)}{dx^2} \le 0$ always holds for $x \ge 0$. The proof of Lemma 2 is completed. ■

Let us take $\phi_{s_iu}^2 \ge \frac{R_{th} s_{s_iu}}{B_t \log_2(1+s_{s_iu})}$ in constraint (37) for example. According to Lemma 2, $\frac{R_{th} s_{s_iu}}{B_t \log_2(1+s_{s_iu})}$ is concave with respect to s_{s_iu}. Define $\boldsymbol{s}^\rho = \{s_{s_iu}^\rho, \forall i\} \bigcup s_{ud}^\rho$ and $\boldsymbol{\phi}^\rho = \{\phi_{s_iu}^\rho, \forall i\} \bigcup \phi_{ud}^\rho$ as two given input sets in the (ρ)th iteration of the SCO. The convex upper-bound of $\frac{R_{th} s_{s_iu}}{B_t \log_2(1+s_{s_iu})}$ can be obtained by the first-order Taylor expansion as follows:

$$\frac{R_{th} s_{s_iu}}{B_t \log_2(1+s_{s_iu})} \le \frac{R_{th} \ln 2}{B_t} \Big(\frac{s_{s_iu}^\rho}{\ln(1+s_{s_iu}^\rho)} + \frac{(1+s_{s_iu}^\rho)\ln(1+s_{s_iu}^\rho) - s_{s_iu}^\rho}{(1+s_{s_iu}^\rho)(\ln(1+s_{s_iu}^\rho))^2} (s_{s_iu} - s_{s_iu}^\rho) \Big). \tag{45}$$

Similarly, since $\phi_{s_iu}^2$ is convex with respect to ϕ_{s_iu}, the concave lower-bound of $\phi_{s_iu}^2$ can be calculated by:

$$\begin{aligned} \phi_{s_iu}^2 &\ge (\phi_{s_iu}^\rho)^2 + 2\phi_{s_iu}^\rho (\phi_{s_iu} - \phi_{s_iu}^\rho) \\ &= 2\phi_{s_iu}^\rho \phi_{s_iu} - (\phi_{s_iu}^\rho)^2. \end{aligned} \tag{46}$$

Lemma 3: Define $h(x,y) = \frac{x}{\sqrt{y}}$. The convex upper-bound of $h(x,y)$ can be calculated by $\sqrt{\frac{y_0}{4x_0^2}} \frac{x^2}{y} + \sqrt{\frac{x_0^2}{4y_0}}$, where (x_0, y_0) is a given local point.

Proof: $h(x,y)$ can be written as $h(x,y) = \sqrt{I(x,y)}$, where $I(x,y) = \frac{x^2}{y}$. Although $h(x,y)$ is not jointly convex with respect to x and y, it is concave with respect to $I(x,y)$.

According to the first-order Taylor expansion, we have:

$$h(x,y) \le \sqrt{I(x_0,y_0)} + \frac{1}{2\sqrt{I(x_0,y_0)}}(I(x,y)-I(x_0,y_0)). \quad (47)$$

Substitute $I(x,y)$ and $I(x_0,y_0)$ to (47), and $\sqrt{\frac{y_0}{4x_0^2}}\frac{x^2}{y}+\sqrt{\frac{x_0^2}{4y_0}}$ is obtained. $I(x,y)$ is a standard quadratic-over-linear function, which is jointly convex with respect to x and y. Thus, $\sqrt{\frac{y_0}{4x_0^2}}\frac{x^2}{y}+\sqrt{\frac{x_0^2}{4y_0}}$ serves as a convex upper-bound of $h(x,y)$. The proof of Lemma 3 is completed. ■

$\boldsymbol{t}^\rho = \{t_{u_i}^\rho, \forall i\}$ is defined as another given input set in the (ρ)th iteration of the SCO. According to Lemma 3, the convex upper-bound of $\sum_{j\in G_v}\frac{s_{ud}}{\sqrt{t_{u_j}}}$ in constraint (36) can be written as:

$$\sum_{j\in G_v}\frac{s_{ud}}{\sqrt{t_{u_j}}} \le \sum_{j\in G_v}\left(\sqrt{\frac{t_{u_j}^\rho}{4(s_{ud}^\rho)^2}}\frac{s_{ud}^2}{t_{u_j}}+\sqrt{\frac{(s_{ud}^\rho)^2}{4t_{u_j}^\rho}}\right). \quad (48)$$

Moreover, $\frac{1}{\sqrt{t_{u_v}}}$ in constraint (36) is convex with respect to t_{u_v}. Similar with (46), its concave lower-bound can be obtained by:

$$\frac{1}{\sqrt{t_{u_v}}} \ge \frac{1}{\sqrt{t_{u_v}^\rho}} - \frac{1}{2\sqrt{(t_{u_v}^\rho)^3}}(t_{u_v}-t_{u_v}^\rho) = \frac{3}{2\sqrt{t_{u_v}^\rho}} - \frac{t_{u_v}}{2\sqrt{(t_{u_v}^\rho)^3}}. \quad (49)$$

In summary, apply the SCO technique to problem (41), and this problem in the (ρ)th iteration can be transformed as:

$$\min_{\boldsymbol{s},\boldsymbol{t},\boldsymbol{\tau},\boldsymbol{\pi},\boldsymbol{\phi},\eta} \quad \eta \quad (50a)$$

$$s.t.\ (35b)\text{-}(35e),\ (39),\ (40), \quad (50b)$$

$$\pi_{u_v} + \sum_{j\in G_v}\left(\sqrt{\frac{t_{u_j}^\rho}{4(s_{ud}^\rho)^2}}\frac{s_{ud}^2}{t_{u_j}}+\sqrt{\frac{(s_{ud}^\rho)^2}{4t_{u_j}^\rho}}\right) \le \frac{3}{2\sqrt{t_{u_v}^\rho}} - \frac{t_{u_v}}{2\sqrt{(t_{u_v}^\rho)^3}}, \quad \forall v,\ \forall i, \quad (50c)$$

$$2\phi_{s_iu}^\rho\phi_{s_iu} - (\phi_{s_iu}^\rho)^2 \ge \frac{R_{th}\ln 2}{B_t}\left(\frac{s_{s_iu}^\rho}{\ln(1+s_{s_iu}^\rho)} + \frac{(1+s_{s_iu}^\rho)\ln(1+s_{s_iu}^\rho)-s_{s_iu}^\rho}{(1+s_{s_iu}^\rho)(\ln(1+s_{s_iu}^\rho))^2}(s_{s_iu}-s_{s_iu}^\rho)\right), \quad \forall i, \quad (50d)$$

$$2\phi_{ud}^\rho\phi_{ud} - (\phi_{ud}^\rho)^2 \ge \frac{R_{th}\ln 2}{B_t}\left(\frac{s_{ud}^\rho}{\ln(1+s_{ud}^\rho)} + \frac{(1+s_{ud}^\rho)\ln(1+s_{ud}^\rho)-s_{ud}^\rho}{(1+s_{ud}^\rho)(\ln(1+s_{ud}^\rho))^2}(s_{ud}-s_{ud}^\rho)\right). \quad (50e)$$

In each iteration, problem (50) is a standard convex optimization problem with a polynomial computational complexity of $O(N_{P_{50}}^{3.5})$, where $N_{P_{50}}$ is the dimension of variables in problem (50). Thus, the total computational complexity of Algorithm 1 is $O(N_c N_{P_{50}}^{3.5})$, where N_c is the iteration number for convergence or equals to the maximum allowed iteration number N_ρ. The objective and all the constraints in problem (50) satisfy the disciplined CVX rules [38]. Problem (50) now can be directly solved using the convex optimization toolbox CVX. Iteratively solving problem (50) gives an optimized upper-bound of problem (41), since the constraints in (36), (37) and (38) are replaced by their corresponding bounds, respectively. The iteration guarantees to converge to a given tolerance error. Our proposed iteration algorithm is summarized in Algorithm 1.

Algorithm 1 The SCO Method for Solving Problem (41)

1. Let $\rho = 0$, and initialize $\boldsymbol{s}_0$, $\boldsymbol{t}_0$ and $\boldsymbol{\phi}_0$;
2. **Repeat**
3. Solve problem (50) with given $\boldsymbol{s}_\rho$, $\boldsymbol{t}_\rho$ and $\boldsymbol{\phi}_\rho$ by using CVX, and obtain the optimal solution denoted by $\boldsymbol{s}_{\rho+1}$, $\boldsymbol{t}_{\rho+1}$ and $\boldsymbol{\phi}_{\rho+1}$;
4. Update $\rho = \rho + 1$;
5. **Until**
6. The min-max outage probability converges to a tolerance error ϵ or the maximum number of iterations N_ρ is reached.

IV. SIMULATION RESULTS

Simulation results are given in this section to verify our proposed algorithm. In this paper, we firstly consider a downlink two-node NOMA scenario included by the Third Generation Partnership Project (3GPP) [36], [37], [39], i.e., $N = 2$. To reveal some regular properties, we firstly assume a symmetric linear network topology as used in [17]–[20]. However, our proposed algorithm can also work with randomly generated coordinates. The coordinates of the BSs and APs used in our simulations are given in Table 1. We adopt the environmental parameters used in [20], [35] as shown in Table 2. The other simulation parameters used in this paper are summarized in Table 3, unless otherwise indicated. For comparison, we design two benchmarks:

TABLE 1. Two pairs of communication nodes.

BSs (m)	APs (m)
$s_1 : (-2000, 0)$	$d_1 : (2000, 0)$
$s_2 : (-1500, 0)$	$d_2 : (1500, 0)$

TABLE 2. Environmental parameters.

a_1	b_1	a_2	b_2	a_3	b_3
$\sqrt{10}$	$\frac{2}{\pi}\ln 10$	-1.5	3.5	44	9

- Benchmark 1 - Power allocation optimization with equal bandwidth allocation, i.e., $\boldsymbol{\beta} = \{\beta_{s_iu} = \beta_{ud} = \frac{1}{N+1}, \forall i\}$.
- Benchmark 2 - Joint bandwidth and power allocation optimization with downlink OMA, where FDMA is

TABLE 3. Simulation parameters.

Parameter	Value
UAV flight radius: r	1000 m
UAV altitude: h	100 m
Maximum allowed transmit power: $P_{\max}$	10 w
Total system bandwidth: B_t	5 MHz
Rate threshold: R_{th}	1 $Mbit/s$
Noise power spectral density: N_0	-174 dBm/Hz
Tolerance error: ϵ	10^{-3}
Maximum number of iterations: N_ρ	20

also applied to the second hops to avoid the co-channel interference.

Note that Benchmark 1 is designed to reveal the reliability gain by the bandwidth allocation between the first and second hops that is not considered in the most of related works. Benchmark 2 is designed to reveal the advantage of downlink NOMA over downlink OMA.

In the step 1 of Algorithm 1, $\boldsymbol{s}_0$, $\boldsymbol{t}_0$ and $\boldsymbol{\phi}_0$ need to be initialized. The equal bandwidth and power allocations are the feasible solution to problem (41). According to (35b), (35d), (37) and (38) as well as the parameters in Table 3, we set $\boldsymbol{t}_0 = \{16, 16\}$, $\boldsymbol{s}_0 = \{2^{\frac{3}{5}} - 1, 2^{\frac{3}{5}} - 1, 2^{\frac{3}{5}} - 1\}$ and $\boldsymbol{\phi}_0 = \{\sqrt{\frac{2^{\frac{3}{5}}-1}{3}}, \sqrt{\frac{2^{\frac{3}{5}}-1}{3}}, \sqrt{\frac{2^{\frac{3}{5}}-1}{3}}\}$, respectively. Figure 2 plots the min-max outage probability versus the number of iterations to show the convergence of our proposed algorithm by iteratively solving problem (50). The min-max outage probability converges to the given tolerance error ϵ. Let us take $\theta = 0.4\pi$ for example, and the sixth iteration leads the min-max outage probability to decrease from 1.106×10^{-4} to 1.105×10^{-4}, which reduces by $0.0904\% < \epsilon$. Thus, the min-max outage probability converges to 1.105×10^{-4} in the sixth iteration.

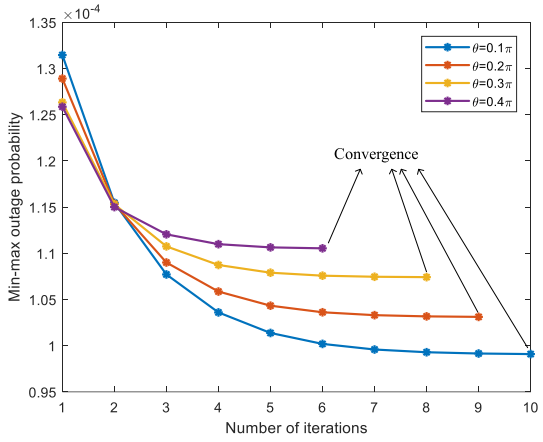

FIGURE 2. Min-max outage probability versus number of iterations.

Figure 3 and Figure 4 plot the bandwidth allocation and power allocation versus the UAV azimuth angle θ, respectively. Figure 5 plots the min-max outage probability versus the UAV azimuth angle θ. Since the time-varying channel is symmetrical about $\theta = \pi$, the bandwidth allocation, power allocation and the min-max outage probability are symmetrical about $\theta = \pi$, respectively. For any given θ, we have $\beta_{s_1u} + \beta_{s_2u} + \beta_{ud} = 1$ and $\xi_{s_1} + \xi_{s_2} + \xi_{u_1} + \xi_{u_2} = 1$. More bandwidth or power resource can provide a higher transmission rate, which reduces the link outage probability. Thus, all the bandwidth and power resources are fully allocated.

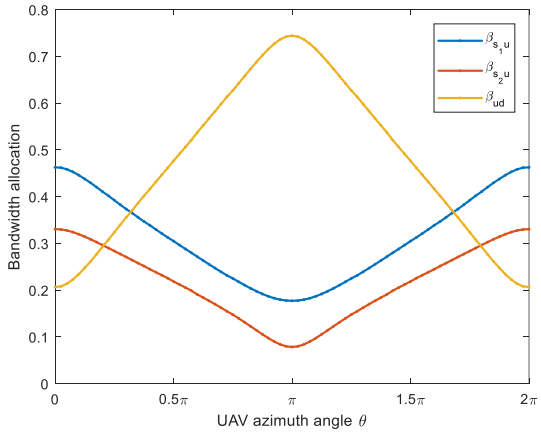

FIGURE 3. Bandwidth allocation versus UAV azimuth angle θ.

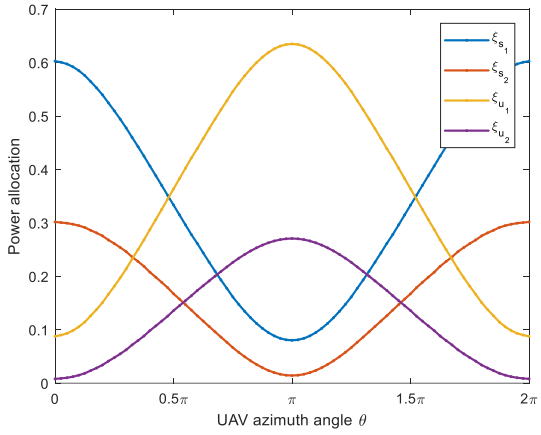

FIGURE 4. Power allocation versus UAV azimuth angle θ.

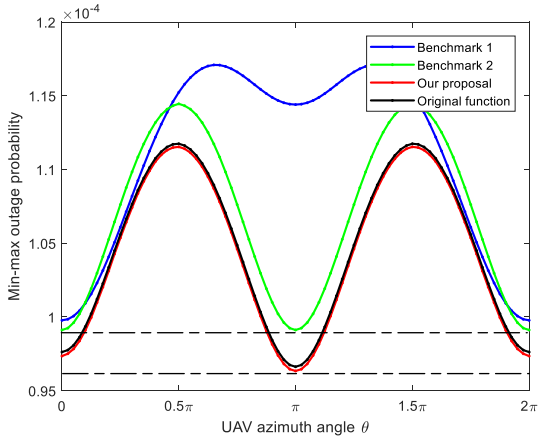

FIGURE 5. Min-max outage probability versus UAV azimuth angle θ.

As θ increases from 0 to π, the UAV gets closer to the BSs. Therefore, the bandwidth and power resources allocated to the BSs decrease and the bandwidth and power resources allocated to the APs increase.

According to Figure 3, β_{ud} is smaller than β_{s_1u} and β_{s_2u} at both sides of the interval $[0, 2\pi]$. This is because the UAV is closer to the APs, which causes the second hops suffer lower path loss than the first hops. More bandwidth resource should be allocated to the first hops to improve the transmission rates of the BSs. Oppositely, β_{ud} is larger than β_{s_1u} and β_{s_2u} around $\theta = \pi$ due to longer distances between the UAV and APs. With any given θ, β_{s_1u} is larger than β_{s_2u}. The distance between BS s_2 and the UAV is smaller than that between BS s_1 and the UAV, thus more bandwidth resource is allocated to link s_1u to reduce the outage probability of this link.

According to Figure 4, at both sides of the interval $[0, 2\pi]$, ξ_{u_1} and ξ_{u_2} are smaller than ξ_{s_1} and ξ_{s_2}, respectively, and the other way around at the middle range of the interval $[0, 2\pi]$. Moreover, ξ_{s_1} is larger than ξ_{s_2} with any given θ. The above two observations can be explained by the similar reasons as used in the bandwidth allocation. For the second hops, ξ_{u_1} is larger than ξ_{u_2} with any given θ. We observe that $d_{ud_1} > d_{ud_2}$ always holds along the UAV trajectory, which means the channel gain of link ud_2 is better than that of link ud_1 according to the channel gain order. As a result, AP d_2 is able to cancel the co-channel interference from link ud_1 by the SIC technique, while AP d_1 suffers the co-channel interference from link ud_2. This leads link ud_1 to obtain more power resource to reduce its outage probability.

Based on the optimized bandwidth and power allocations, the original outage probability is also calculated according to (22). Figure 5 shows at the majority of θ values, the min-max outage probability obtained by the first-order asymptotic outage probability can well match that obtained by the original outage probability. This verifies the efficiency of the first-order asymptotic outage probability. Since Benchmark 1 only optimizes the power allocation with equal bandwidth allocation, the joint optimization of the bandwidth and power allocations by our proposed algorithm can achieve a lower min-max outage probability. From Figure 3, the bandwidth allocation difference first decreases and then increases with θ increasing from 0 to π. Thus, the gap between our proposed algorithm and Benchmark 1 follows the similar trend, and more reliability gain occurs around $\theta = \pi$. Although Benchmark 2 jointly optimizes the bandwidth and power allocations, the min-max outage probability based on downlink OMA is still higher than that based on downlink NOMA. The second hops share the same bandwidth resource by using downlink NOMA, which introduces the co-channel interference. However, a part of the co-channel interference can be canceled according to the channel gain order, which improves the bandwidth utilization. Thus, the reliability performance by using downlink NOMA outperforms that by using downlink OMA. The time-varying channel is symmetrical about $\theta = 0.5\pi$ by using downlink OMA. According to Benchmark 2, the min-max outage probability is also symmetrical about $\theta = 0.5\pi$. However, by using downlink NOMA, the min-max outage probability is not symmetrical about $\theta = 0.5\pi$ due to the existence of the co-channel interference in the second hops. A lower min-max outage probability is obtained when $\theta = \pi$. The UAV is closer to the BSs with $\theta = \pi$, thus more bandwidth and power resources should be allocated to the second hops. As a result, the bandwidth utilization can be further improved by using the SIC technique. Figure 5 also shows even using downlink NOMA, the equal bandwidth allocation scheme for the first and second hops sometimes causes worse system reliability than using downlink OMA.

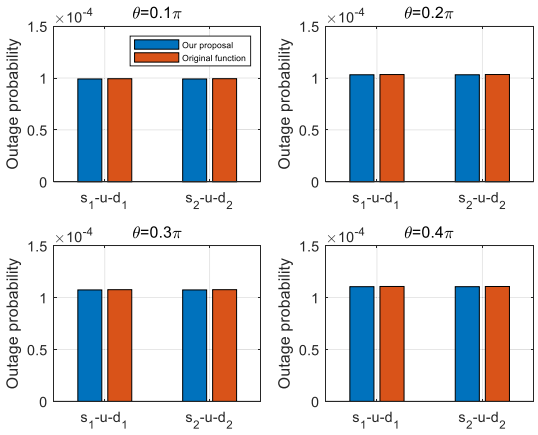

FIGURE 6. Outage probability fairness among all links.

Figure 6 shows the outage probability fairness among all links for four possible UAV locations. The min-max outage probability is obtained when different links have the same outage probability. Otherwise, the maximum outage probability can be further reduced by decreasing the outage probability gap among all links. Therefore, the first-order asymptotic outage probability among all links obeys the strict fairness by our proposed algorithm. Since the first-order asymptotic outage probability is close to the original outage probability at majority of θ values, the original outage probability fairness among all links can also be approximately achieved.

In order to further reveal the global reliability gain of our proposed algorithm, we also investigate the overall average outage probability η_o versus the total transmit power $P_{\max}$ as shown in Figure 7. We divide the interval $[0, \pi]$ into 41 samples to quantitatively calculate the value of η_o as follows:

$$\eta_o = \frac{1}{41}\sum_{n=1}^{41}\eta_{\min}[0.025\pi(n-1)], \tag{51}$$

where $\eta_{\min}[0.025\pi(n-1)]$ represents the corresponding min-max outage probability with $\theta = 0.025\pi(n-1)$. As $P_{\max}$ increases, the overall average outage probability by our proposed algorithm decreases. This is because $P_{i,out}$ in (22) is negatively related to $P_{\max}$. Moreover, our proposed algorithm has a lower overall average outage probability compared with our designed two benchmarks. Figure 8 plots the overall average outage probability versus the rate threshold R_{th}.

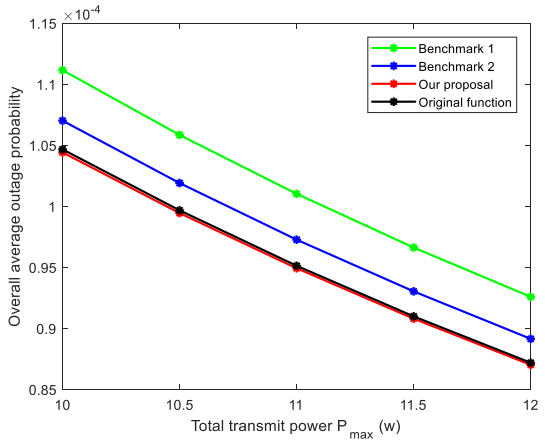

FIGURE 7. Overall average outage probability versus total transmit power P_{max}.

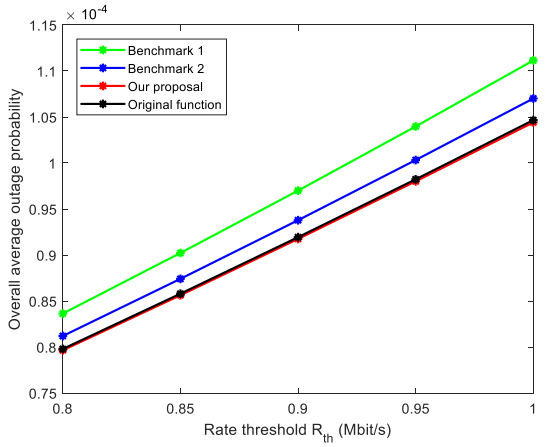

FIGURE 8. Overall average outage probability versus rate threshold R_{th}.

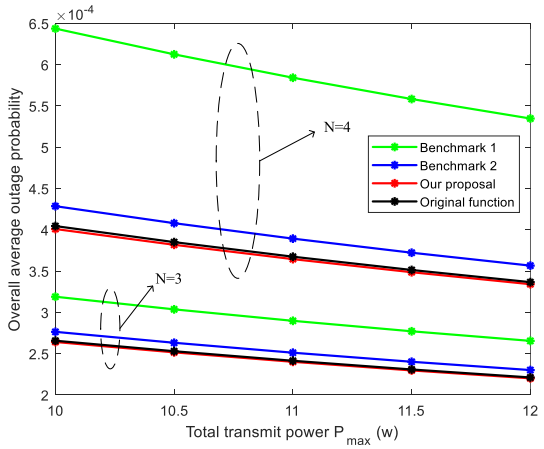

FIGURE 9. Overall average outage probability versus total transmit power P_{max} with random nodes distribution.

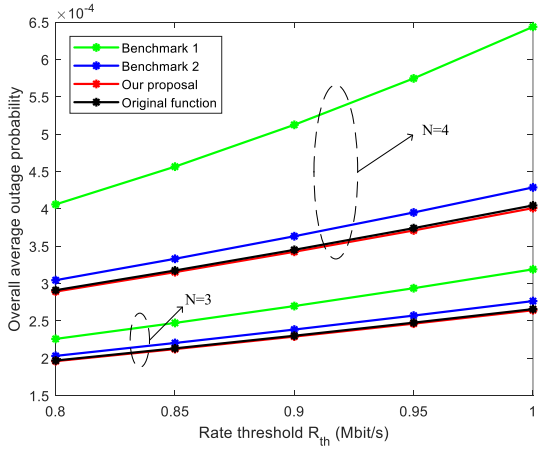

FIGURE 10. Overall average outage probability versus rate threshold R_{th} with random nodes distribution.

According to (22), the overall average outage probability is increasing with respect to R_{th}. The reliability gain can also be obtained by our proposed algorithm from Figure 8.

Finally, we verify our proposed algorithm with random nodes distribution. For downlink multi-node NOMA, it can be efficiently accomplished by node grouping with each group containing an odd or even number of nodes [32]. Thus, we perform our simulations for another two basic cases with more links, i.e., an odd number of links with $N = 3$ and an even number of links with $N = 4$. The BSs are randomly distributed in a rectangular region with vertex coordinates $(-2500, 100)$, $(-1500, 100)$, $(-1500, -100)$ and $(-2500, -100)$. The APs are randomly distributed in a rectangular region with vertex coordinates $(1500, 100)$, $(2500, 100)$, $(2500, -100)$ and $(1500, -100)$. Each BS randomly pre-matches with one AP. For each case, $\boldsymbol{s}_0$, $\boldsymbol{t}_0$ and $\boldsymbol{\phi}_0$ in the step 1 of Algorithm 1 need to be re-initialized due to more variables. A common initialization method is to assume equal power allocation, then adjust the bandwidth that is allocated to the second hops to satisfy the SIC constraint in (18). Based on this method and according to the variable substitutions in (32), (33) and (34), we re-initialize $\boldsymbol{t}_0 = \{36, 36, 36\}$, $\boldsymbol{s}_0 = \{2^3 - 1, 2^3 - 1, 2^3 - 1, 2^{\frac{1}{4}} - 1\}$ and $\boldsymbol{\phi}_0 = \{\sqrt{2^3 - 1}, \sqrt{2^3 - 1}, \sqrt{2^3 - 1}, \sqrt{2^{\frac{1}{4}} - 1}\}$ with $N = 3$. Similarly, we re-initialize $\boldsymbol{t}_0 = \{64, 64, 64, 64\}$, $\boldsymbol{s}_0 = \{2^4 - 1, 2^4 - 1, 2^4 - 1, 2^4 - 1, 2^{\frac{1}{4}} - 1\}$ and $\boldsymbol{\phi}_0 = \{\sqrt{2^4 - 1}, \sqrt{2^4 - 1}, \sqrt{2^4 - 1}, \sqrt{2^4 - 1}, \sqrt{2^{\frac{1}{4}} - 1}\}$ with $N = 4$. Figure 9 shows the overall average outage probability versus the total transmit power $P_{\max}$ with random nodes distribution. Figure 10 shows the overall average outage probability versus the rate threshold R_{th} with random nodes distribution. Each simulation result in Figure 9 and Figure 10 is averaged over 50 random realizations. A larger number of nodes result in a higher overall average outage probability due to a limited communication resource. However, from Figure 9, more reliability gain is obtained with a larger N by our proposed algorithm. This is due to the fact that more links share the bandwidth equipped for the second hops by using downlink NOMA, which helps to further improve the bandwidth utilization through the SIC. Similar observations can be obtained from Figure 10. Figure 7, Figure 8, Figure 9

and Figure 10 also imply the accuracy between the first-order asymptotic outage probability and the original outage probability.

V. CONCLUSION

This paper has investigated a UAV-enabled mobile relaying system where a UAV flies in a circular trajectory to provide wireless access for remaining APs in an emergency situation. To improve the system reliability, we have jointly optimized the bandwidth and power allocations along the UAV trajectory by using downlink NOMA, aiming to minimize the maximum outage probability among all links. We have proposed an iteration algorithm based on the SCO technique to solve our formulated problem. Simulation results have shown the reliability gain by our proposed algorithm.

Note that this work optimizes the resource allocation to improve the system reliability by only applying downlink NOMA to the UAV. The joint use of uplink and downlink NOMA transmissions to optimize the resource allocation is another interesting direction. Moreover, joint UAV trajectory and NOMA resource allocation optimization is another way to further improve the system reliability for UAV-enabled multiple source-destination relaying.

APPENDIX
THE PROOF OF CONCAVE-CONVEX PROPERTY

According to the term $(2^{\frac{R_{th}}{B_I \beta_{ud}}} - 1)\sum_j \xi_{u_j}$ in constraint (18), we define a similar function as $g_1(x, y) = (2^{\frac{1}{x}} - 1)y = g_2(x, y) - y$, where $g_2(x, y) = 2^{\frac{1}{x}} y$. The Hessian matrix of $g_2(x, y)$ can be written as:

$$\boldsymbol{H}_1 = \begin{bmatrix} \frac{mqy(2x+m)}{x^4} & -\frac{mq}{x^2} \\ -\frac{mq}{x^2} & 0 \end{bmatrix}, \tag{52}$$

where $q = 2^{\frac{1}{x}}$ and $m = \ln 2$. The two eigenvalues of $\boldsymbol{H}_1$ can be written as:

$$e_1 = \frac{mq(my+2xy+\sqrt{4x^4+4x^2y^2+4mxy^2+m^2y^2})}{2x^4}, \tag{53}$$

$$e_2 = \frac{mq(my+2xy-\sqrt{4x^4+4x^2y^2+4mxy^2+m^2y^2})}{2x^4}. \tag{54}$$

$e_1 \geq 0$ for any $x \geq 0$ and $y \geq 0$. Besides, we have:

$$(my + 2xy)^2 - (4x^4 + 4x^2y^2 + 4mxy^2 + m^2y^2) = -4x^4 \leq 0, \tag{55}$$

i.e., $e_2 \leq 0$ for any $x \geq 0$ and $y \geq 0$. Therefore, $g_2(x, y)$ is non-convex with respect to x and y, which implies that the constraint in (18) for successful SIC is non-convex.

According to $F_{2,i}$, we define another similar function as $Q_1(x, y, z) = \frac{(2^{\frac{1}{x}}-1)x}{y-(2^{\frac{1}{x}}-1)z}$. Let $\boldsymbol{H}_2$ be the Hessian matrix of $Q_1(x, y, z)$. Since $\boldsymbol{H}_2$ is complex with x, y and z, it is omitted for saving space. The determinant of $\boldsymbol{H}_2$ is given by:

$$|\boldsymbol{H}_2| = \frac{2m^2q^2(1-q)^3}{x(y-(q-1)z)^7} \leq 0. \tag{56}$$

(56) implies that $F_{2,i}$ is non-convex with respect to β_{ud}, ξ_{u_v} and ξ_{u_j}.

REFERENCES

[1] S. Hayat, E. Yanmaz, and R. Muzaffar, "Survey on unmanned aerial vehicle networks for civil applications: A communications viewpoint," *IEEE Commun. Surveys Tuts.*, vol. 18, no. 4, pp. 2624–2661, Apr. 2016.

[2] Z. Hu, Z. Bai, Y. Yang, Z. Zheng, K. Bian, and L. Song, "UAV aided aerial-ground IoT for air quality sensing in smart city: Architecture, technologies, and implementation," *IEEE Netw.*, vol. 33, no. 2, pp. 14–22, Mar. 2019.

[3] F. Qi, X. Zhu, G. Mang, M. Kadoch, and W. Li, "UAV Network and IoT in the Sky for Future Smart Cities," *IEEE Netw.*, vol. 33, no. 2, pp. 96–101, Mar. 2019.

[4] Y. Zeng, R. Zhang, and T. J. Lim, "Wireless communications with unmanned aerial vehicles: Opportunities and challenges," *IEEE Commun. Mag.*, vol. 54, no. 5, pp. 36–42, May 2016.

[5] C. Zhang, W. Zhang, W. Wang, L. Yang, and W. Zhang, "Research challenges and opportunities of UAV millimeter-wave communications," *IEEE Wireless Commun.*, vol. 26, no. 1, pp. 58–62, Feb. 2019.

[6] A. Al-Hourani, S. Kandeepan, and A. Jamalipour, "Modeling air-to-ground path loss for low altitude platforms in urban environments," in *Proc. IEEE Global Commun. Conf.*, Dec. 2014, pp. 2898–2904.

[7] A. Jaziri, R. Nasri, and T. Chahed, "Congestion mitigation in 5G networks using drone relays," in *Proc. Int. Wireless Commun. Mobile Comput. Conf. (IWCMC)*, Sep. 2016, pp. 233–238.

[8] J. Lyu, Y. Zeng, and R. Zhang, "Spectrum sharing and cyclical multiple access in UAV-aided cellular offloading," in *Proc. IEEE Global Commun. Conf.*, Dec. 2017, pp. 1–6.

[9] J. Lyu, Y. Zeng, and R. Zhang, "UAV-aided offloading for cellular hotspot," *IEEE Trans. Wireless Commun.*, vol. 17, no. 6, pp. 3988–4001, Jun. 2018.

[10] L. Zhu, J. Zhang, Z. Xiao, X. Cao, D. O. Wu, and X.-G. Xia, "3-D beamforming for flexible coverage in millimeter-wave UAV communications," *IEEE Wireless Commun. Lett.*, vol. 8, no. 3, pp. 837–840, Jun. 2019.

[11] A. Fotouhi, M. Ding, and M. Hassan, "Service on demand: Drone base stations cruising in the cellular network," in *Proc. IEEE Globecom Workshops (GC Wkshps)*, Dec. 2017, pp. 1–6.

[12] G. Tuna, T. V. Mumcu, and K. Gulez, "Design strategies of unmanned aerial vehicle-aided communication for disaster recovery," in *Proc. High Capacity Opt. Netw. Emerg./Enabling Technol.*, Dec. 2012, pp. 115–119.

[13] A. Merwaday and I. Guvenc, "UAV assisted heterogeneous networks for public safety communications," in *Proc. IEEE Wireless Commun. Netw. Conf. Workshops (WCNCW)*, Mar. 2015, pp. 329–334.

[14] J. Cui, H. Shakhatreh, B. Hu, S. Chen, and C. Wang, "Power-efficient deployment of a UAV for emergency indoor wireless coverage," *IEEE Access*, vol. 6, pp. 73200–73209, 2018.

[15] A. Kumbhar, I. Guvenc, S. Singh, and A. Tuncer, "Exploiting LTE-advanced hetnets and FeICIC for UAV-assisted public safety communications," *IEEE Access*, vol. 6, pp. 783–796, 2018.

[16] N. Zhao, W. Lu, M. Sheng, Y. Chen, J. Tang, F. R. Yu, and K.-K. Wong, "UAV-assisted emergency networks in disasters," *IEEE Wireless Commun.*, vol. 26, no. 1, pp. 45–51, Feb. 2019.

[17] F. Ono, H. Ochiai, and R. Miura, "A wireless relay network based on unmanned aircraft system with rate optimization," *IEEE Trans. Wireless Commun.*, vol. 15, no. 11, pp. 7699–7708, Nov. 2016.

[18] X. Jiang, Z. Yin, Z. Wu, Z. Yang, and J. Sun, "Outage probability optimization for UAV-enabled wireless relay networks in fading channels," *Phys. Commun.*, vol. 33, pp. 35–45, Apr. 2019.

[19] Q. Song, S. Jin, and F.-C. Zheng, "Joint power allocation and beamforming for UAV-enabled relaying systems with channel estimation errors," in *Proc. IEEE 87th Veh. Technol. Conf. (VTC Spring)*, Jun. 2018. pp. 1–5.

[20] Q. Song, F.-C. Zheng, Y. Zeng, and J. Zhang, "Joint beamforming and power allocation for UAV-enabled full-duplex relay," *IEEE Trans. Veh. Technol.*, vol. 68, no. 2, pp. 1657–1671, Feb. 2019.

[21] Q. Yuan, Y. Hu, C. Wang, and Y. Li, "Joint 3D beamforming and trajectory design for UAV-enabled mobile relaying system," *IEEE Access*, vol. 7, pp. 26488–26496, 2019.

[22] S. Zhang, H. Zhang, Q. He, K. Bian, and L. Song, "Joint trajectory and power optimization for UAV relay networks," *IEEE Commun. Lett.*, vol. 22, no. 1, pp. 161–164, Jan. 2018.

[23] S. Zeng, H. Zhang, K. Bian, and L. Song, "UAV relaying: Power allocation and trajectory optimization using decode-and-forward protocol," in *Proc. IEEE Int. Conf. Commun. Workshops (ICC Workshops)*, May 2018, pp. 1–6.
[24] M. Hua, Y. Wang, Z. Zhang, C. Li, Y. Huang, and L. Yang, "Outage probability minimization for low-altitude UAV-enabled full-duplex mobile relaying systems," *China Commun.*, vol. 15, no. 5, pp. 9–24, May 2018.
[25] P. K. Sharma and D. I. Kim, "UAV-enabled downlink wireless system with non-orthogonal multiple access," in *Proc. IEEE Globecom Workshops*, Dec. 2017, pp. 1–6.
[26] M. M. Selim, M. Rihan, Y. Yang, L. Huang, Z. Quan, and J. Ma, "On the outage probability and power control of D2D underlaying NOMA UAV-assisted networks," *IEEE Access*, vol. 7, pp. 16525–16536, 2019.
[27] A. Han, T. Lv, and X. Zhang, "Outage performance of NOMA-based UAV-assisted communication with imperfect SIC," in *Proc. IEEE Wireless Commun. Netw. Conf. (WCNC)*, Apr. 2019. pp. 1–6.
[28] T. Hou, Y. Liu, Z. Song, X. Sun, and Y. Chen, "Multiple antenna aided NOMA in UAV networks: A stochastic geometry approach," *IEEE Trans. Commun.*, vol. 67, no. 2, pp. 1031–1044, Feb. 2019.
[29] X. Wang, H. Zhang, K. J. Kim, Y. Tian, and A. Nallanathan, "Performance analysis of cooperative aerial base station-assisted networks with non-orthogonal multiple access," *IEEE Trans. Wireless Commun.*, vol. 18, no. 12, pp. 5983–5999, Dec. 2019.
[30] J. Li, Y. Liu, X. Li, C. Shen, and Y. Chen, "Non-orthogonal multiple access in cooperative UAV networks: A stochastic geometry model," in *Proc. IEEE 90th Veh. Technol. Conf. (VTC-Fall)*, Sep. 2019, pp. 1–6.
[31] Z. Xiao, L. Zhu, J. Choi, P. Xia, and X.-G. Xia, "Joint power allocation and beamforming for non-orthogonal multiple access (NOMA) in 5G millimeter wave communications," *IEEE Trans. Wireless Commun.*, vol. 17, no. 5, pp. 2961–2974, May 2018.
[32] L. Zhu, J. Zhang, Z. Xiao, X. Cao, D. O. Wu, and X.-G. Xia, "Millimeter-wave NOMA with user grouping, power allocation and hybrid beamforming," *IEEE Trans. Wireless Commun.*, vol. 18, no. 11, pp. 5065–5079, Nov. 2019.
[33] Y. Zeng, J. Xu, and R. Zhang, "Energy minimization for wireless communication with rotary-wing UAV," *IEEE Trans. Wireless Commun.*, vol. 18, no. 4, pp. 2329–2345, Apr. 2019.
[34] Y. Zeng and R. Zhang, "Energy-efficient UAV communication with trajectory optimization," *IEEE Trans. Wireless Commun.*, vol. 16, no. 6, pp. 3747–3760, Jun. 2017.
[35] M. M. Azari, F. Rosas, K.-C. Chen, and S. Pollin, "Ultra reliable UAV communication using altitude and cooperation diversity," *IEEE Trans. Commun.*, vol. 66, no. 1, pp. 330–344, Jan. 2018.
[36] X. Wang, J. Wang, L. He, and J. Song, "Outage analysis for downlink NOMA with statistical channel state information," *IEEE Wireless Commun. Lett.*, vol. 7, no. 2, pp. 142–145, Apr. 2018.
[37] Z. Yang, Z. Ding, P. Fan, and Z. Ma, "Outage performance for dynamic power allocation in hybrid non-orthogonal multiple access systems," *IEEE Commun. Lett.*, vol. 20, no. 8, pp. 1695–1698, Aug. 2016.
[38] M. C. Grant and S. P. Boyd. (2014). *The CVX Users Guide, Release 2.1*. [Online]. Available: http://cvxr.com/cvx/doc/CVX.pdf
[39] *Study Downlink Multiuser Superposition Transmission for LTE*, Gener. Partnership Project, Shanghai, China, Mar. 2015.

LEI WANG received the master's degree in communication and information systems from the Kunming University of Science and Technology (KMUST), China, in 2016. He is currently pursuing the Ph.D. degree with the State Key Laboratory of Networking and Switching Technology, Beijing University of Posts and Telecommunications (BUPT), China. His current research interests include future wireless mobile communication networks and unmanned aerial vehicle (UAV) networks.

BO HU (Member, IEEE) received the Ph.D. degree of communications and information systems from the Beijing University of Posts and Telecommunications (BUPT), in 2006. He is currently a Professor with the State Key Laboratory of Networking and Switching Technology, BUPT. He has published over 80 research articles in international journals & conferences and coauthored three books. He is active in the ITU-T SG13 for international standards and focuses on the mobility management and machine learning for IMT-2020(5G) & beyond. His research interests include integrated satellite and terrestrial mobile communication systems for B5G and 6G, network artificial intelligence, and mobility management & control.

SHANZHI CHEN (Fellow, IEEE) received the bachelor's degree from Xidian University, in 1991, and the Ph.D. degree from the Beijing University of Posts and Telecommunications, China, in 1997. He joined the Datang Telecom Technology and Industry Group and the China Academy of Telecommunication Technology (CATT), in 1994, and has been serving as the EVP of Research and Development, since 2008. He is currently the Director of the State Key Laboratory of Wireless Mobile Communications, CATT, where he conducted research and standardization on 4G TD-LTE and 5G. He has authored and coauthored four books, including the well-known textbook *Mobility Management: Principle, Technology and Applications* (Springer Press), 17 book chapters, more than 100 journal articles, 50 conference papers, and over 50 patents in these areas. He has contributed to the design, standardization, and development of 4G TD-LTE and 5G mobile communication systems. His current research interests include 5G mobile communications, network architectures, vehicular communication networks, and the Internet of Things. He served as a member and a TPC Chair of many international conferences. His achievements have received multiple top awards and honors by China central government, especially the Grand Prize of the National Award for Scientific and Technological Progress, China, in 2016 (the highest Prize in China). He is the Area Editor of the IEEE Internet of Things, the Editor of the IEEE Network, and the Guest Editor of the IEEE Wireless Communications, the IEEE Communications Magazine, and the IEEE Transactions on Vehicular Technology.

JIAN CUI received the master's degree from the Shandong University of Science and Technology, in 2014. He is currently pursuing the Ph.D. degree with the State Key Laboratory of Networking and Switching Technology, Beijing University of Posts and Telecommunications (BUPT), China. His research interests include future wireless communication networks and unmanned aerial vehicle (UAV) networks.